

Photothermal Beam Deflection and Photoaction Spectroscopic Study of CdS Photoelectrodes in Polysulfide Electrolyte

ROBERT E. WAGNER and ANDREAS MANDELIS*

Photoacoustic and Photothermal Sciences Laboratory, Department of Mechanical Engineering (R.E.W.); and Laser and Light-wave Research Center, University of Toronto, Toronto M5S 1A4, Canada (A.M.)

A number of experimental photothermal deflection, ac photovoltage, and ac photocurrent spectra for CdS photoelectrochemical cells are presented. The spectra were obtained under various conditions, with the use of modulated light: open circuit and short circuit, and with a dc bias applied across the working and counter electrodes. The measurement of both the photothermal deflection and the photoaction signals allows one to monitor two energy conversion channels, namely optical-to-thermal, and optical-to-electrical. The photothermal deflection technique was found to provide useful information regarding the surface condition of the electrodes, with respect to polishing or corrosion damage. Finally, the effect of a current-induced species gradient at the working electrode/electrolyte interface upon the photothermal deflection signal is also examined.

Index Headings: Photothermal deflection spectroscopy; Photocurrent/photovoltage spectroscopy; CdS photoelectrode; Photoelectrochemical energy conversion.

INTRODUCTION

CdS, a direct-gap II–VI compound semiconductor, has been the subject of many photoelectrochemical^{1,2} and optical studies;^{3–5} both solid-state⁶ and solid/electrolyte^{1,2} junction devices employing CdS have been built which efficiently convert high energy light ($h\nu > 2.4$ eV) to electrical energy. CdS is an electronically complex material, but tends to be *n*-type; donor levels are usually the result of impurity doping, but can even be plentiful in pure materials due to the wide variety of possible native defects.⁷ In this study involving four CdS crystals, both pure and doped materials were used, with resistivities varying over a wide range.

When CdS (or any other suitable semiconductor) is brought into contact with an electrolyte (usually concentrated), a depletion layer is formed within the semiconductor surface, and a photovoltaic effect occurs when the semiconductor/electrolyte junction is illuminated with superbandgap light—the basis for the photoelectrochemical cell.⁸ If a second metal (counter) electrode is placed in the electrolyte with the semiconductor, and an insulated metal ohmic contact is made on the semiconductor back, the photovoltaic effect can be measured as the open-circuit voltage. Alternatively, a dc bias can be applied across the illuminated working electrode (WE) and the dark counter electrode (CE); the dc bias will induce both a shift in the electronic bands within the semiconductor and a dark cell current, while the light will create a photocurrent, flowing under essentially short-circuit conditions. Both of these arrangements are com-

monly used to study the optoelectronic properties of semiconductor/electrolyte junctions.

The performance of a given photoelectrochemical (PEC) cell will depend upon both the optical and the electronic properties of the junction interface. The traditional method for obtaining the optical properties of a semiconductor electrode is to perform transmission and/or reflectivity measurements. These techniques are not well suited for thick, light-scattering crystals, especially when the samples are mounted in an electrochemical cell and immersed in electrolyte. When optical absorption measurements are to be carried out *in situ*, with the PEC electrode operating as a photovoltaic device, clearly other spectroscopic techniques are required. One convenient way of obtaining qualitative optical absorption spectra for PEC electrodes is to use photothermal deflection spectroscopy (PDS), a well-known thermal wave technique.⁹ PDS is a noncontact technique which employs a probe laser beam propagating parallel to the WE surface to detect the refractive index (temperature) gradient which exists perpendicular to an illuminated electrode; most of the light absorbed by the WE is normally converted to heat by the efficient nonradiative de-excitation of the nonequilibrium, optically generated electron-hole pairs. For signal-to-noise ratio enhancement, the optical excitation is usually periodically modulated, and the ac component of the PDS signal is monitored via lock-in detection. In this regime the PDS technique can be used to obtain depth-resolved information, by varying the modulation frequency; for instance, at higher frequencies the PDS amplitude and phase provide insight regarding near-surface absorption. Surface information is important in PEC studies because the interface properties of an electrode will often determine the efficiency of its operation; surface polishing damage or thin corrosion layers which form during cell operation can both cause the deterioration of cell performance. One problem in applying PDS to a PEC cell under load occurs when the cell current creates a species gradient along the probe beam path; this species gradient causes a refractive index gradient which will perturb the thermal PDS signal component. A spectrum will be examined which was considerably altered by a species gradient.

Both the optical and electronic characteristics of a PEC electrode can be studied by obtaining photoaction (photocurrent/voltage) spectra under various cell conditions, i.e., at open circuit (OC) or short circuit (SC), or under dc bias. In the majority of cases, we obtained photoaction spectra concurrently with PDS spectra, in which case both the amplitude and phase were obtained

Received 28 April 1988; revision received 12 August 1988.

* Author to whom correspondence should be sent.

for the ac photocurrent/photovoltage. Owing to the lack of pertinent theoretical models for ac optical excitation, discussion of photoaction phase spectra will be entirely descriptive. Overall, the photoaction spectra were consistent with the electrode optical and electronic properties obtained by other means (PDS and Mott-Schottky analysis).

EXPERIMENTAL

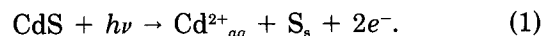
For the sake of brevity, the four CdS samples will now be referred to by the following labels: (1) pure high resistivity, HR-CdS; (2) pure low resistivity, LR-CdS; (3) F-doped, F-CdS; and (4) Ga-doped, Ga-CdS. All four crystals were obtained from Eagle-Picher, Inc. (Miami, OK). Since all samples were grown from high-temperature melts or vapors, they were assumed to have the wurtzite hexagonal structure. The HR- and LR-CdS samples were grown by the chemical vapor transport method described elsewhere.¹⁰ The doped materials (F- and Ga-CdS) were grown by crystal pulling from a melt in a carbon crucible, with the dopants present in the melt. All of the crystals were of *n*-type, which is almost always the case for CdS.⁷

The HR-CdS crystal measured $10 \times 9 \times 0.5$ mm³, and its exposed face was parallel to its optic axis; its nominal resistivity was 1.93×10^5 Ω cm.¹¹ The LR-CdS sample measured $10 \times 10 \times 0.5$ mm³ and also had its optic axis parallel to its exposed face; its nominal resistivity was 4.75 Ω cm.¹¹ Originally the HR and LR crystals were 2 mm thick, but they were polished down to one-quarter of their original thickness in an alumina-water slurry. The F-CdS crystal contained 0.01% F¹¹ and measured $9 \times 6 \times 1.5$ mm³; its exposed face was of unknown orientation. Fluorine atoms are known to form donors when incorporated into the CdS lattice.¹² The Ga-CdS sample contained 100 ppm Ga¹¹ and measured $10 \times 10 \times 2$ mm³; it was also of unknown orientation. Gallium atoms are also known to form donors in CdS.¹² Both of these doped samples were cut from cylindrical boules with the use of a thin, diamond-edged, copper circular saw and polished in an alumina-water slurry. The pure samples were known to be single crystals, but the doped samples were cut from boules of unknown quality and were not positively identified as single crystals.

Several steps were required to build operational working electrodes from the polished crystals. First, the crystals were etched in 3 M HCl in order to remove as much of the surface damage layer as possible; the 20-second etch was followed by a rinse in distilled water. Second, a bead of semiliquid indium-gallium amalgam was rubbed onto the back of each crystal, opposite the face which was to be exposed to the electrolyte. Smith¹³ has shown that simple pressure contact results in a good ohmic junction between the In-Ga mixture and the CdS crystal. Third, each crystal was epoxied (Devcon, 5 minute) onto an acrylic backing so that all surfaces of the crystal except the front face would be insulated. Finally, a copper wire was contacted to the In-Ga bead on each crystal back via a hole in the acrylic backing; this contact was then insulated by filling the access hole with epoxy. The working electrodes were periodically etched in HCl to remove corrosion products. The PEC cell counter electrode, a

piece of platinum foil covered in Pt black in order to increase its effective surface area, had a projected surface area of about 6 cm²; the Pt electrode seemed to be inert in the corrosive polysulfide electrolyte. The potential of the WE was monitored with respect to a saturated calomel electrode (SCE).

With respect to our choice of cell electrolyte, we decided upon a polysulfide solution. Our electrolyte was expected to satisfy several requirements: Photoanodic corrosion of the electrode should be inhibited; this type of corrosion leads to the formation of a passivating sulfur layer on the crystal when anodic current is passed through the electrode under illumination.



The electrolyte should also be transparent to the light which is used to excite the electrode, and the electrolyte should provide a reversible redox reaction whereby the species oxidized at one electrode would be reduced at the other. According to the Ellis *et al.*^{1,2} and Karas and Ellis,¹⁴ polysulfide electrolyte (Na₂S, S, and NaOH in distilled water) was found to quench the anodic corrosion of CdS up to a certain current density; also, under steady current flow the electrolyte composition remained fairly constant. Unfortunately, the large amount of sulfur (1.5 M S to 1.0 M Na₂S) recommended by Hodes¹⁵ to stop corrosion would yield a solution opaque to the shorter visible wavelengths. Taking the above factors into account, we employed two similar polysulfide electrolytes: (1) 1.0 M Na₂S, 0.01 M S, and 1 M NaOH in distilled water proved to be quite transparent; and (2) 1.0 M Na₂S, 0.05 M S, and 1 M NaOH in distilled water was more opaque than the former solution, but it provided better corrosion protection. The two solutions will henceforth be referred to as 0.01 M PS and 0.05 M PS, respectively. The solutions were prepared from: (1) sodium sulfide, 9-hydrate crystal (Na₂S·9H₂O), J. T. Baker, "Baker Analyzed"; (2) sublimed sulfur powder, U.S.P., J. T. Baker; (3) sodium hydroxide pellets (NaOH), 98.3% NaOH, J. T. Baker, "Baker Analyzed"; and (4) distilled water. After the completion of our work we discovered a paper by Licht and Manassen¹⁶ which claimed that NaOH does not serve any useful purpose in the polysulfide electrolyte and can be excluded from the solution. Polysulfide electrolytes are known to decompose in air, and should be argon purged to remove dissolved oxygen; we did not purge our solutions, but they were kept in airtight containers and discarded after a few days of use.

The three cell electrodes and the electrolyte were contained in an airtight acrylic cell. The cell featured three windows, one to allow the entry of the exciting optical beam and two to allow the entry and exit of the PDS probe laser beam. Other important parts of the experimental apparatus are as follows: Optical excitation was carried out by means of an Oriel 8540 1000-W xenon lamp in an Oriel 6141 housing; the lamp was equipped with a photofeedback system to stabilize its power output. The lamp output was focused onto the input aperture of an Instruments S.A. Inc. monochromator, equipped with a diffraction grating blazed in the infrared. The 4-mm monochromator slits provided an optical bandwidth of about 16 nm. The lamp beam from the monochromator was periodically modulated with a

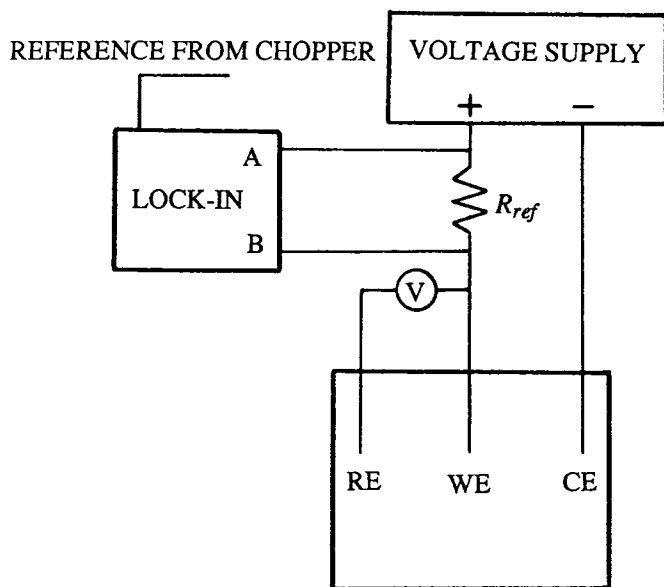


FIG. 1. ac Photocurrent vs. voltage apparatus; R_{ref} , known reference resistor.

PRA OC 4000 mechanical chopper. Three UV-grade lenses, two $f = 80$ mm plano-convex and an $f = 50$ mm bi-convex, were used to focus the lamp beam to a rectangular image of a few mm^2 . All devices except the lamp were mounted on a Newport Research Inc. optical table.

The PDS probe beam was provided by an Optikon 2-mW He-Ne laser, LGK 7672, with an Optikon LM2P power supply. An $f = 20$ mm plano-convex lens focused the probe beam as it passed over the WE. The probe laser was mounted on a tilting gimbal to allow careful alignment of the beam relative to the sample surface. The PDS beam deflection was detected by a United Detector Technology 431 X-Y position monitor, equipped with a UDT SC/25 quad-cell; this detector was covered by a 632.8-nm (He-Ne wavelength) interference filter to minimize noise due to stray excitation light. The UDT 431 signal was fed into an Ithaco 1201 low-noise pre-amplifier for amplification and filtering. The ac signal from the pre-amp was then fed into an EG&G Princeton Applied Research Model 5204 lock-in analyzer. The lock-in output, in this and in other cases, was sampled by a computer-driven analog-to-digital conversion board.

The ac open-circuit photovoltage (OC PV) was monitored by connecting the WE and CE leads directly to the A and B inputs, respectively, of a lock-in. The ac short-circuit photocurrent (SC PC) was measured in a similar fashion, but a small (about $10\ \Omega$) reference resistor was connected across the A and B inputs of the lock-in. The ac photocurrent-bias apparatus (see Fig. 1) consisted of a Solartron Schlumberger 1250 frequency response analyzer connected across a series combination of a reference resistor (about $10\ \Omega$) and the PEC cell. The ac photocurrent across the reference resistor was monitored with a lock-in.

RESULTS AND DISCUSSION

PDS Spectra of CdS in Distilled Water. Prior to obtaining spectra in polysulfide electrolyte, we obtained the PDS spectra of the CdS samples in distilled water

(DW). Although various means have been developed for determining the absolute optical absorption coefficient of a sample from PDS measurements (see, for instance, Mandelis¹⁷), in the present case PDS data will only be used to provide an indication of the relative bandgaps of the four crystals. Also, the ability of the PDS phase measurements to detect surface layer absorption will be emphasized. Generally, the PDS signal amplitude and phase for a homogeneous semiconductor obey the following spectral behavior: (1) Strongly absorbed superbandgap photons result in a relatively large magnitude and small phase lag. The PDS signal is approximately a linear function of the absorption coefficient when the absorption length is greater than the thermal diffusion length (see Eq. 2). When the absorption length is less than the thermal diffusion length, the PDS signal is termed to be saturated, and the amplitude and phase are insensitive, nonlinear functions of the absorption coefficient. (2) As the photon energy is decreased towards the bandgap energy, the magnitude decreases and the phase lag increases; and (3) subbandgap photons are usually absorbed weakly by bulk defect states, resulting in a small magnitude and large phase lag. Quantitatively, one expects to see a phase shift of about 45° as the absorption coefficient varies from large to small values. If a thin, defect-rich damage layer exists on the crystal surface due to polishing or corrosion, for instance, the subbandgap PDS magnitude will generally increase, and the subbandgap phase lag will decrease, compared to that of a damage-free sample, indicating absorption near the surface. Furthermore, if substantial absorption occurs in the sample backing, phase shifts larger than 45° can be expected (for example, see the experimental data for the related photopyroelectric spectroscopy of CdS, in Mandelis *et al.*,¹⁸ Fig. 3b).

All CdS PDS amplitude spectra were normalized by a reference lamp spectrum obtained by measuring the PDS spectrum of a black-painted glass slide. In addition, some spectra (both PDS and photoaction) were smoothed in order to attenuate spectral features due to noise and imperfect normalization; spectra containing distinct, sharp spectral features were not smoothed, since such a process would distort the spectra considerably. The smoothing was carried out by replacing each data point in a spectrum with new values obtained by averaging each point with its two adjacent data values; all spectra which were smoothed have been indicated as such.

Before we start examining the PDS spectra in detail, note that in order to compare spectra of different crystals we must obtain spectra at the same modulation frequency and take into account the variations in sample thickness. For instance, Fig. 2 shows two PDS amplitude spectra for F-CdS in DW obtained at 11 and 79 Hz; the optical band edge for this sample appears to be a function of modulation frequency, which is clearly not the case. The apparent band edge shift was actually due to the decrease in the sample thermal diffusion length, μ_t , as the frequency was increased:

$$\mu_t = (2k/\rho C\omega)^{1/2} \quad (2)$$

where k is the thermal conductivity, ρ is the density, C is the specific heat, of the sample, and ω is the angular frequency. This aspect of thermal wave spectroscopies

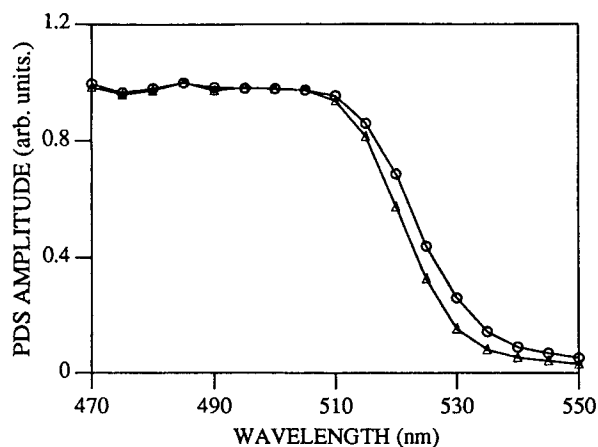


FIG. 2. OC PDS amplitude spectra of F-CdS in DW; 11 (o) and 79 (Δ) Hz.

has been discussed by Fesquet *et al.*¹⁹ in their paper on determining the absorption coefficient of thick samples using photoacoustic spectroscopy. Figure 2 also illustrates the depth-profiling nature of PDS—namely, that the strong, near-surface absorption becomes relatively more important than bulk absorption as the modulation frequency increases.

Figure 3 (F-CdS, 25 Hz) shows typical PDS amplitude and phase behavior: For $\lambda < 500$ nm the absorption coefficient (α) is relatively constant, about 10^5 cm⁻¹,³⁻⁵ resulting in an almost constant magnitude and phase. As α begins to drop, the heating “centroid” moves deeper into the crystal bulk, the magnitude drops, and the phase lag becomes larger. A simulation of the PDS signal for CdS at 25 Hz, using the model due to Mandelis,¹⁷ indicated that the PDS signal was grossly saturated for $\alpha > 5 \times 10^3$ cm⁻¹; thus, the significant drop in the PDS amplitude for $\lambda > 500$ nm would not be initiated until $\alpha < 5 \times 10^3$ cm⁻¹. The small, residual PDS amplitude for $\lambda > 540$ nm was probably due to a combination of weak bulk absorption, surface absorption, and absorption in the backing; the subbandgap phase behavior should help in the interpretation of the amplitude data. The phase lag increased 30° from 505 to 540 nm, after which it remained constant until 580 nm. This phase change was close to the 32° predicted by the model due

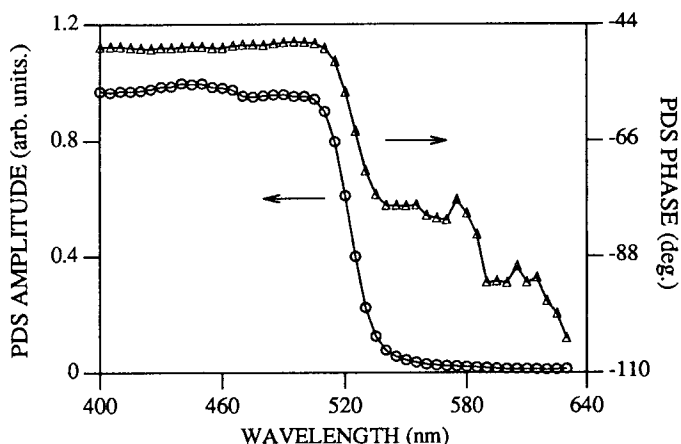


FIG. 3. OC PDS amplitude (o) and phase (Δ) spectra of F-CdS in DW; 25 Hz; smoothed.

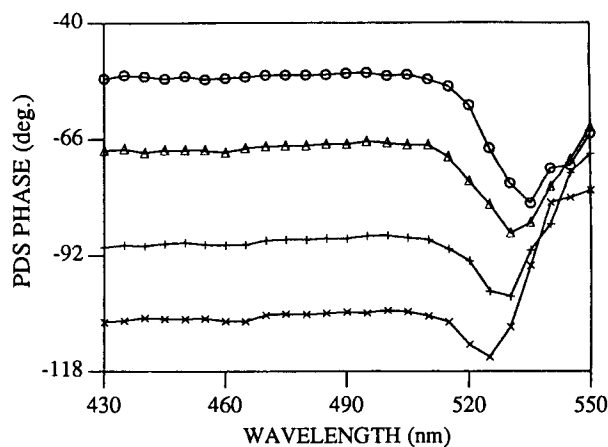


FIG. 4. OC PDS phase spectra of LR-CdS in DW; 11 (o), 25 (Δ), 49 (+), and 79 (\times) Hz; smoothed.

to Mandelis,¹⁷ for a large change in α , pointing to bulk absorption as the dominant signal source below 580 nm. Beyond 580 nm, the phase lag increased a further 25°, indicating that backing absorption may have been responsible for this signal. With regard to the signal-to-noise ratio (SNR) for PDS measurements, the amplitude SNR was >100 and >10 , and the phase standard deviation was $<0.5^\circ$ and $<5^\circ$, in the superbandgap and subbandgap regions, respectively.

In contrast to the spectra of Fig. 3, the PDS phase spectra for the LR-CdS (Fig. 4) showed strong evidence for substantial surface absorption: Following the expected phase lag increase at the band edge, the phase lag was observed to decrease substantially at longer wavelengths, an indication that surface absorption provided a significant component to the subbandgap PDS signal.^{20,21} As the modulation frequency was increased, the subbandgap phase lag decreased relative to the superbandgap phase, and the turning point was blue-shifted, suggesting that surface absorption became the dominant source of subbandgap signal at higher frequency. The origin of the strong surface absorption could have been a damage layer caused by crystal polishing; the LR-CdS had been polished considerably and then etched prior to mounting. If the etch was not complete, a significant number of defects would be left within the crys-

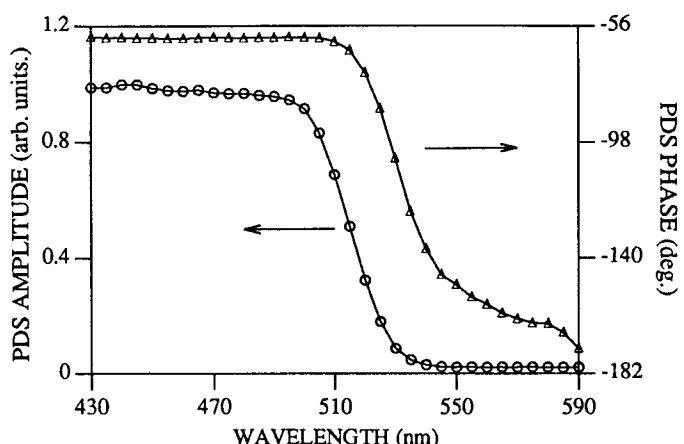


FIG. 5. OC PDS amplitude (o) and phase (Δ) spectra of HR-CdS in DW; 25 Hz; smoothed.

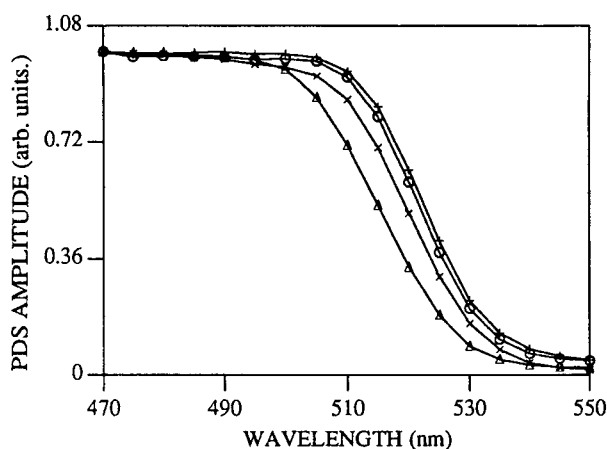


FIG. 6. OC PDS amplitude spectra in DW; 25 Hz; Ga-CdS (o), HR-CdS (Δ), F-CdS (+), and LR-CdS (\times); smoothed.

tal surface, giving rise to electronic states in the crystal bandgap. This same crystal also gave a Mott-Schottky plot with features attesting to a damage layer; after the sample was re-etched, both the Mott-Schottky plot and PDS phase spectra evinced that minimal surface damage was present.²²

The HR-CdS PDS amplitude and phase spectra (Fig. 5) were slightly different from those of the other samples, in that the amplitude band edge was blue-shifted 15 nm relative to the phase band edge, while they were coincident for the three low-resistivity materials. Also, the phase was very constant for $\lambda < 510$ nm, whereas the low-resistivity samples showed a gentle rise within this region; the reasons for these differences in the high- and low-resistivity phase behaviors are not known. The large phase lag increase across the band edge ($> 100^\circ$ at 25 Hz) suggests that the subbandgap signal may have been derived mainly from absorption in the backing. Considerable thermal communication can be expected between the back and front of the crystal at 25 Hz, because the thermal diffusion length (0.44 mm) is close to the sample thickness (0.5 mm).

The PDS amplitude spectra of all four CdS samples in distilled water have been plotted in Fig. 6. The HR-CdS appears to have the largest bandgap, while of the low-resistivity samples, the LR-CdS has a bandgap midway between that of the HR-CdS and the Ga-CdS and F-CdS samples. These spectra are consistent with the existence of electronic defect states in the bandgaps of the low-resistivity samples; these states provide additional levels for optical transitions, effectively decreasing the optical bandgaps of these samples if the donor levels are sufficient in quantity, and lie near the conduction band edge, as is usually the case. Defect states would tend to alter the absorption spectrum of a defect-free material most significantly at lower absorption coefficients, a spectral region where the PDS spectrum would not be grossly saturated. We calculated²² the donor densities (N_d) of the low-resistivity crystals from manufacturer's specifications,¹¹ and found that N_d (m^{-3}) for the LR-CdS, Ga-CdS, and F-CdS were 6.26×10^{21} , 4.02×10^{24} , and 2.01×10^{24} , respectively. Assuming the apparent bandgap decrease in a sample is proportional to its donor density, the relative positions of the band edges

shown in Fig. 6 are reasonable. Note that all of the samples were thermally thick (thickness greater than μ_t) at 25 Hz, and that all were optically thick for absorption coefficients above 20 cm^{-1} . Also, the wide bandpass of the monochromator (16 nm) may have resulted in spectra which were distorted to some extent.

It should be noted that a certain amount of corrosion appeared to occur under illumination in distilled water, even at open circuit. The small illuminated region of the crystal took on a mat appearance, while the rest of the sample remained glossy. Gurevich and Pleskov²³ point out that, if only part of the crystal is illuminated, this region will corrode, while the dark region will support cathodic reactions like hydrogen evolution or the reduction of dissolved oxygen.

CdS PEC Corrosion Under Short-Circuit Conditions. Before any spectra obtained under SC conditions are examined, it would be useful to point out that a certain amount of corrosion was observed to occur when photocurrents were initiated at a fresh crystal surface. The degree of surface corrosion was simply monitored by measuring the photocurrent (PC) as a function of time: The usual PC decay pattern consisted of a quick initial drop, after which an asymptote was reached. From this observation it appears that the reversible redox reaction became dominant over the corrosion reaction after the current density had been reduced somewhat by the formation of a corrosion layer, a result consistent with rotating ring-disk measurements made by Heller and Miller.²⁴ Thus, when spectra were recorded under SC conditions, a certain amount of time was allowed for the current to reach a steady value before data were taken. Overall, corrosion was found to be more severe in the 0.01 M PS than in the 0.05 M PS, a result in agreement with the work of Hodes.¹⁵

The Effect of Ionic Species Gradients on the PDS Signal. When current is flowing through the WE, a gradient of ionic species will form in the electrolyte adjacent to the electrode. Due to the relatively slow rate of ionic diffusion, the species gradient will be quite stationary when the current flow is modulated at typical PDS frequencies (> 10 Hz); note that the ionic diffusion coefficients for a selection of strong electrolytes listed in the *CRC Handbook of Chemistry and Physics*²⁵ range from 10^{-5} to $3 \times 10^{-5} \text{ cm}^2\text{s}^{-1}$, while the thermal diffusivity ($=k\rho/C$, where k is thermal conductivity, ρ is density, and C is specific heat), the thermal counterpart of the ionic diffusion coefficient, is about $1.5 \times 10^{-3} \text{ cm}^2\text{s}^{-1}$ for water²⁶—in other words, heat diffusion is a much faster process than ionic diffusion. Ionic species gradients are important because they can deflect a probe laser beam in the same manner as a temperature gradient.²⁷ In fact, Dorthe-Merle *et al.*²⁸ and Pawliszyn *et al.*²⁹ have experimentally observed laser beam deflection signals due to both species and temperature gradients.

Now, consider the case where the PEC cell current is modulated at a typical PDS frequency (> 10 Hz), producing both temperature and species gradients; as already noted, the ac component of the species gradient will be very small at these frequencies, although the dc component will be quite large. Thus, the ac PDS signal will be almost entirely due to the temperature gradient. This does not mean that the species gradient has no

significant bearing upon the PDS signal; in fact, the species gradient will cause a dc deflection of the probe beam, which in turn, affects the ac PDS signal through its strong dependence on the beam offset value. For instance, if the species gradient causes the probe beam to deflect away from the electrode, the PDS signal will be rapidly decreased.

Evidence for the existence of a species gradient effect was obtained as follows: A PEC electrode (LR-CdS in 0.01 M PS) was illuminated with dc light, and the dc PDS deflection was recorded as a function of wavelength, at open circuit and short circuit. The resulting wavelength spectra were qualitatively similar, both showing large signals for superbandgap light ($\lambda < 525$ nm). The key difference between the two spectra was that the OC spectrum showed much smaller signals than the SC spectrum for comparable light intensities; since similar amounts of heat were generated at OC and SC (as evidenced by the ac PDS signals), there must have been a nonthermal mechanism responsible for the large dc PDS signal at SC. An ionic species gradient can be used to explain the enhanced SC PDS signal: At OC no current was flowing, so no species gradient existed (except for the minor Helmholtz and Gouy-Chapman layers); at SC a current was present and a species gradient was formed. The combination of the species and temperature gradients may have resulted in the large dc PDS deflection.

Further evidence for the species gradient effect was obtained by monitoring the time dependence of the PDS signal. For instance, when a PC was initiated in an LR-CdS/0.01 M PS system, a significant change in the PDS signal was observed (Fig. 7). First, the PDS signal dropped quickly; this decrease was probably associated with the initial formation of the species gradient, which would tend to push the probe beam away from the WE.²⁷ After about eight minutes, the PDS signal began to increase; this trend was possibly related to the current decay, which decreased the species gradient, allowing the PDS probe beam to move closer to the sample. The PDS phase behavior in Fig. 7 further supports the theory that a species gradient was responsible for the PDS signal time dependence. Note that the phase mirrors the amplitude: For instance, as the amplitude decreases, the phase lag becomes larger; this behavior is representative of a probe beam whose offset from the WE is increasing. Likewise, when the amplitude increases, the phase lag decreases, again an indication of probe beam offset diminution. Keeping the preceding points in mind, we are ready to discuss the nature of PDS spectra obtained under OC and SC conditions.

The Normalization of Photoaction Spectra. In the first subsection under "Results and Discussion," several normalized PDS spectra were presented; the normalization process was quite straightforward, owing to the linear dependence of the PDS signal upon excitation intensity and to the absence of solution absorption. On the other hand, we have previously found²² that both the OC PV and the SC PC follow a wide range of functional dependences upon illumination power, depending upon the absorption coefficient, the surface condition, and the actual power levels employed. Therefore, the normalization of photoaction spectra to remove lamp spectral features is not as simple as in the PDS case.

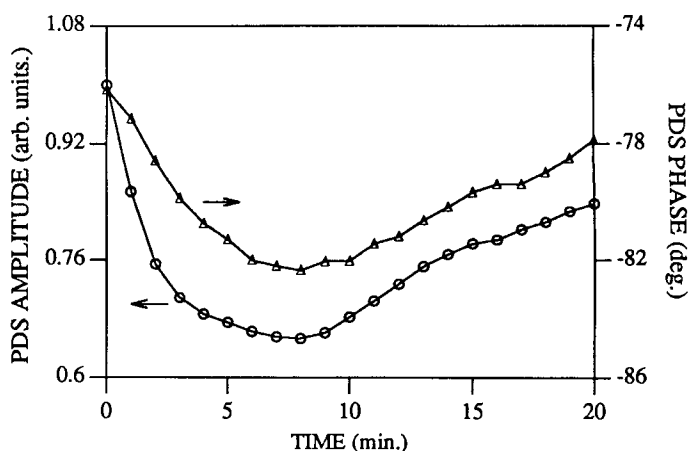


FIG. 7. SC PDS amplitude (o) and phase (Δ) vs. time for LR-CdS in 0.01 M PS; 490 nm; 25 Hz; smoothed.

The normalization procedure for spectra obtained in 0.01 M PS was as follows: Generally, these spectra were taken over the range of 430 to 590 nm. Owing to the fact that the lamp spectrum was quite flat over the 470–590 nm span, the normalization process suitability was judged by how well the <470-nm drop-off in lamp intensity was removed from a given photoaction spectrum. By trial-and-error we found that the photoaction amplitude spectra were purged of lamp spectral features by the use of an $I_0(\lambda)$ or $I_0(\lambda)^{1/2}$ normalization, where $I_0(\lambda)$ represents the PDS lamp spectrum.

In 0.05 M PS, data were taken over the 470–590 nm range; the normalization process was similar to the one described above, but was of less significance due to the spectral flatness of the band in question. The 0.05 M PS was found to absorb considerable light below 500 nm, but spectra were not corrected for solution absorption. Overall, regardless of the method employed, the normalization process did not obscure the important information contained within a spectrum, namely, the shape and location of the apparent band edge and the relative importance of the subbandgap signal. All spectra have been labeled according to the normalization employed.

On a final note, we have also found²² that the PV and PC phase are also dependent upon intensity, to varying degrees; thus, phase spectra considered to have structure related to lamp intensity variations will be pointed out.

PDS and Photoaction Spectra of CdS Electrodes in Polysulfide Electrolyte, Obtained Under OC and SC Conditions. In the majority of cases, PDS and photoaction spectra were obtained in both 0.01 M and 0.05 M PS, and at two different modulation frequencies, namely, 25 and 79 Hz. With regard to the PDS spectra, the apparent band edges of the four crystals seemed to be independent of solution: Distilled water, 0.01 M PS, and 0.05 M PS yielded almost identical amplitude spectra. Also, the subbandgap PDS phase behavior in 0.01 M PS indicated surface absorption to a much greater extent than was the case for the 0.05 M PS, consistent with the increased incidence of photocorrosion, and hence damage layer formation, in 0.01 M PS. Furthermore, PDS amplitude spectra obtained under SC conditions were often perturbed relative to the OC spectra by the presence of current-induced species gradients. For instance, Fig. 8

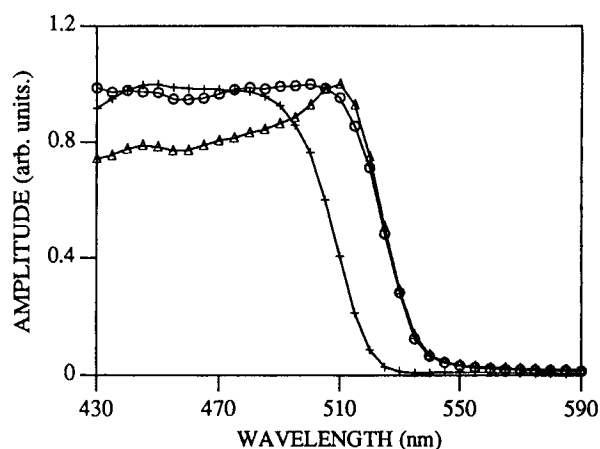


FIG. 8. OC PDS (o), SC PDS (Δ), and SC PC (+) amplitude spectra of F-CdS in 0.01 M PS; 25 Hz; PC normalized by $I_0(\lambda)^{1/2}$; smoothed.

shows the SC PDS, SC PC, and OC PDS amplitude spectra for F-CdS in 0.01 M PS. Note that the SC PDS amplitude curve is attenuated relative to the OC PDS curve, over the range 430 to 500 nm, which corresponds to the span over which the PC was largest. Small PDS phase shifts were also observed in the high PC spectral regions, and the shifts were consistent with the pattern previously outlined above, in the third subsection under "Results and Discussion."

In addition, there were a few cases in which the sub-bandgap PDS phase lag was found to be smaller than the superbandgap phase lag (for example, Fig. 9a). This type of behavior can be explained in the following manner: Consider an electrode with an optically thin surface-damage layer, the absorption coefficient of which is considerably larger than that of the bulk at subbandgap wavelengths (of the bulk). Thus, regardless of the wavelength of the exciting light, most of the illumination passes through the damage layer to the crystal bulk. Also, the reasonable assumption can be made that the disordered damage layer has a much smaller thermal conductivity than the bulk crystal. Now under conditions where the exciting light is strongly absorbed by the bulk, the measured PDS phase lag is larger than it would be if no damage layer had been present, because the heat must diffuse through the poorly heat conducting damage layer to reach the electrolyte. On the other hand, when the bulk absorption coefficient is much smaller than that of the damage layer (i.e., the subbandgap region), the surface becomes the main heat generating source; since absorption in the surface layer occurs physically closer to the solid/electrolyte interface than does absorption in the bulk crystal, the phase lag is not as large as was the case for superbandgap light. In Fig. 9b one can see the effect of modulation frequency upon the information contained in the subbandgap PDS phase. At 25 Hz, the crystal showed no evidence of surface absorption; in fact, the large phase shift across the band edge pointed to subbandgap absorption in the backing. On the other hand, at 79 Hz, when the PDS method was more sensitive to surface absorption, the subbandgap phase clearly indicated the presence of surface absorption. This type of behavior, which was observed for several different samples under a wide variety of cell conditions, demonstrates

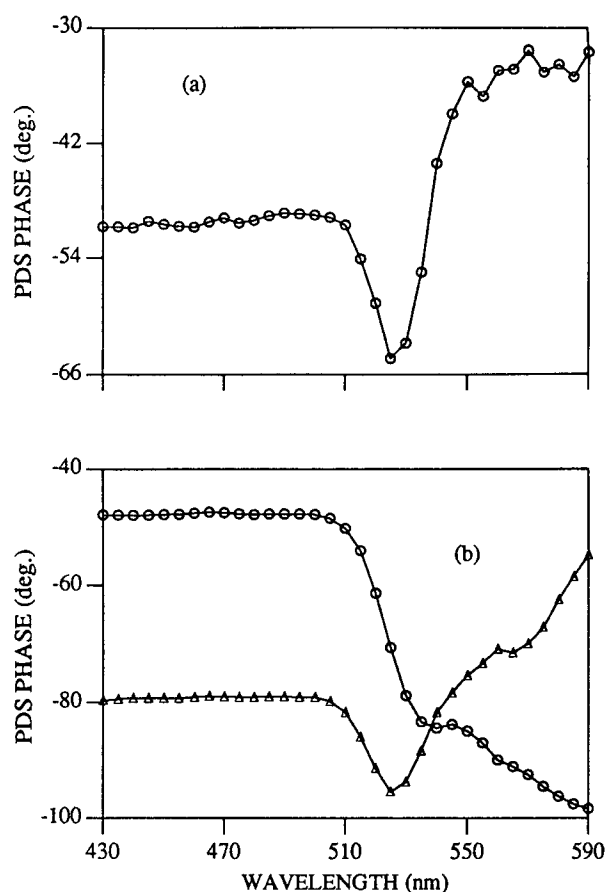


FIG. 9. (a) OC PDS phase spectrum of LR-CdS in 0.01 M PS; 25 Hz; and (b) OC PDS phase spectra of HR-CdS in 0.01 M PS; 25 (o) and 79 (Δ) Hz; smoothed.

the importance which the thermal diffusion length plays in allowing one to detect or monitor surface absorption.

With regard to the photoaction spectra, let us now discuss the OC PV and SC PC amplitude spectra. First, unlike the PDS response, in both cases the spectra obtained at 25 and 79 Hz were very similar. Second, the apparent PV and PC band edges of each crystal were normally quite coincident, and were shifted relative to the PDS band edge; the extent of this shift can be seen by referring to Fig. 8. When the OC PV and SC PC spectra for the four crystals were plotted together, a common pattern emerged: As can be seen in Fig. 10 (OC PV amplitude spectra, 0.05 M PS, 25 Hz), the HR-CdS and the heavily doped Ga-CdS had PV band edges at the longest and shortest wavelengths, respectively. This pattern is opposite the one obtained for the PDS spectra, in which a band edge was situated at longer wavelengths as the doping-density was increased. The above-noted trend in PV and PC band edge locations is in agreement with the Gartner model,³⁰ an elementary model for the SC PC in which the minority carrier transport equation is solved for the neutral bulk region of a Schottky barrier device. This model predicts that, as the donor density increases and the depletion layer becomes thinner, carriers generated by low absorption coefficient light outside the depletion layer are collected less efficiently, effectively shifting the PC (or PV) band edge to higher absorption coefficients (shorter wavelengths). Although the

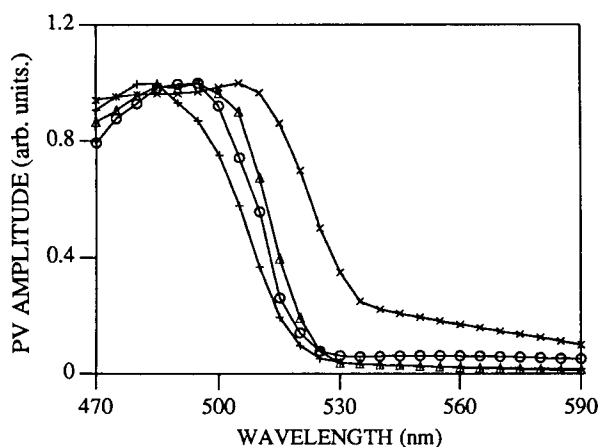


FIG. 10. OC PV amplitude spectra in 0.05 M PS; 25 Hz; F-CdS (o), LR-CdS (Δ), Ga-CdS (+), and HR-CdS, smoothed (\times); all spectra normalized by $I_0(\lambda)^{1/2}$, except Ga-CdS($I_0(\lambda)$).

HR-CdS had PV and PC band edges at the longest wavelength, at shorter wavelengths this material yielded short-circuit quantum efficiencies five to ten times smaller than those of the low-resistivity materials: The poor quantum efficiency in the high-resistivity sample can be attributed to the weak built-in field which exists throughout the sample,³¹ in contrast to the large field which comprises the depletion layer of a low-resistivity electrode. Several electrochemical measurements²² were performed which indicated the absence of a depletion layer in the HR-CdS. In addition, the HR-CdS PC spectra were found to be affected, in the superbandgap region, by the presence of the He-Ne probe beam: Apparently, some of the probe beam entered the low free carrier density sample, and induced carrier photoexcitation which altered this density (see Gerischer *et al.*³¹).

Roger *et al.*³² have also observed a shift between the apparent PDS and PC band edges for a CuInSe₂ electrode; they related the shift to the fact that the PDS thermal diffusion length (about 10^{-4} m) was much longer than the electron diffusion length (about 10^{-6} m), which causes different depths of the sample to be probed by the two methods. The Gartner model³⁰ does predict that, as the hole diffusion length is increased (in CdS), the PC band edge will be situated at longer wavelengths; owing to a lack of knowledge regarding the carrier diffusion lengths of the four CdS samples employed in this study, it is unclear how important this effect was in determining the PC and PV band edge locations.

Enhanced surface absorption seemed to provide a significant relative subbandgap OC PV, but not an SC PC. An explanation for the poor PC could be as follows: For each photon absorbed at the surface, assume that one free carrier was generated, with its pair carrier localized in a bandgap state. The free carrier would be mobile enough to induce a voltage at OC, but little current would flow at SC because the carriers localized in gap states would have limited mobility. The generation of a PV merely requires the separation of the electron-hole pair, and is not totally impeded if one of the carriers is in a localized state; on the other hand, it is necessary that both carriers be mobile if a PC is to flow, since surface holes are required for the WE anodic reaction, and re-

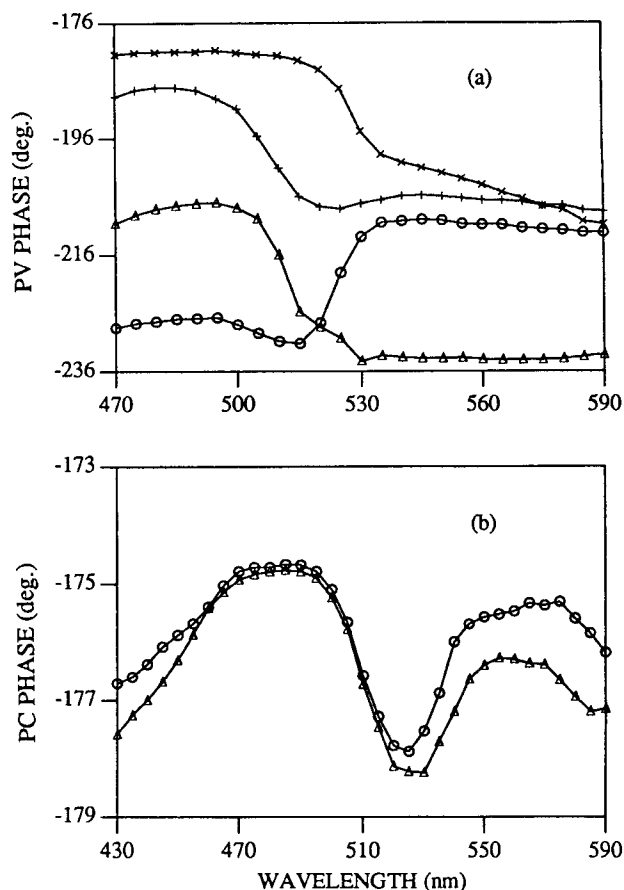


FIG. 11. (a) OC PV phase spectra in 0.05 M PS; 25 Hz; F-CdS (o), LR-CdS (Δ), Ga-CdS (+), and HR-CdS (\times), and (b) SC PC phase spectra of F-CdS in 0.01 M PS; 25 (o) and 79 (Δ) Hz; smoothed.

ducing electrons are needed at the CE—clearly one of these two reactions will be compromised if either the electron or the hole is localized.

The photoaction phase spectra were somewhat more difficult to interpret, owing to the wide variability in observed behavior. Figure 11a depicts the OC PV phase spectra of the four materials in 0.05 M PS; the data obtained in 0.01 M PS are not shown. Several observations can be drawn from Fig. 11a. First, all spectra were quite similar in form, showing an approximately 20° shift near the crystal band edges. The curves obtained in 0.01 M PS were relatively more complex: The magnitudes of the band edge shifts were quite variable, and phase changes across the band edge were not always monotonic. The irregular behavior in the 0.01 M PS may have been related to the surface corrosion layers which were more likely to reach considerable thickness in the 0.01 M PS; the "well-behaved" curves obtained in 0.05 M PS were possibly indicative of a clean crystal surface. Second, in 0.05 M PS, the doped samples (Ga- and F-CdS) showed subbandgap ($\lambda > 515$ nm) phase up-turns (much more obvious for the F-CdS), which were not present for the pure samples—these upturns may be indicative of large defect densities. The variability of phase behavior for a given sample in different solutions seems to indicate that the phase is affected just as much by surface properties as by bulk electronic properties.

With regard to the PC phase spectra depicted in Fig.

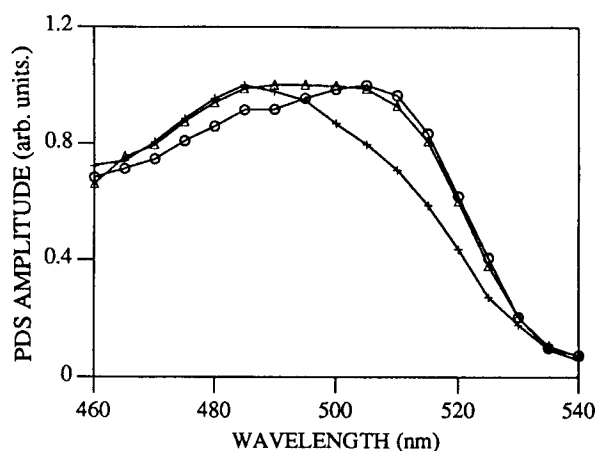


FIG. 12. PDS amplitude spectra of Ga-CdS, under various biases, in 0.05 M PS; 25 Hz; -1.51 (o), $+0.40$ (Δ), and $+2.19$ (+) V/SCE.

11b, it is apparent that the PC band edge phase shifts were considerably smaller than the PV phase shifts. The PC phase spectral features can be explained as follows: First, the <470 -nm drop correlated exactly with the lamp spectrum; second, the 495–520 nm dip was probably associated with the crystal band edge; and third, the broad peak centered at 560 nm also reflected the lamp spectrum. One can see that the interpretation of PC phase spectra was made more difficult due to the intensity-dependence of the phase.

The photoaction phase spectra did not change dramatically as the modulation frequency was changed from 25 to 79 Hz; usually the super- and subbandgap regions of the spectrum shifted up or down in unison, to varying degrees, as the frequency was changed.

Overall, the examination of OC PV and SC PC phase spectra to obtain information about the properties of a PEC electrode is currently speculative, owing to the dearth of theoretical models which realistically predict the photoaction phase behavior. We can qualitatively state that the surface properties of an electrode probably play a major role in determining the phase behavior as the sample band edge is traversed.

PDS and PC Spectra of CdS in Polysulfide Electrolyte, Obtained with a dc Bias Applied Across the WE and CE. PDS and PC spectra were obtained concurrently, at various dc biases, for the three low-resistivity electrodes in both 0.01 M and 0.05 M PS, at 25 Hz. The three measurement biases were chosen to be evenly spaced, with one at a forward bias, one at a small reverse bias, and one at a larger reverse bias.

With regard to the PDS measurements, the apparent PDS band edges for the three samples were relatively independent of bias, as expected. Observed bias variations in the superbandgap region of the PDS amplitude spectra can be explained with the aid of the following expression for the PDS signal as a function of bias, adapted from the work of Fujishima *et al.*:³³

$$\text{PDS}(V) = K_1 h\nu + K_2 Q(V + K_3) \quad (3)$$

where Q is the photocurrent quantum efficiency, $h\nu$ is the photon energy, V is the applied potential vs. SCE, and K_1 , K_2 , and K_3 are wavelength-independent parameters. Equation 3 indicates that as the bias, V , is made

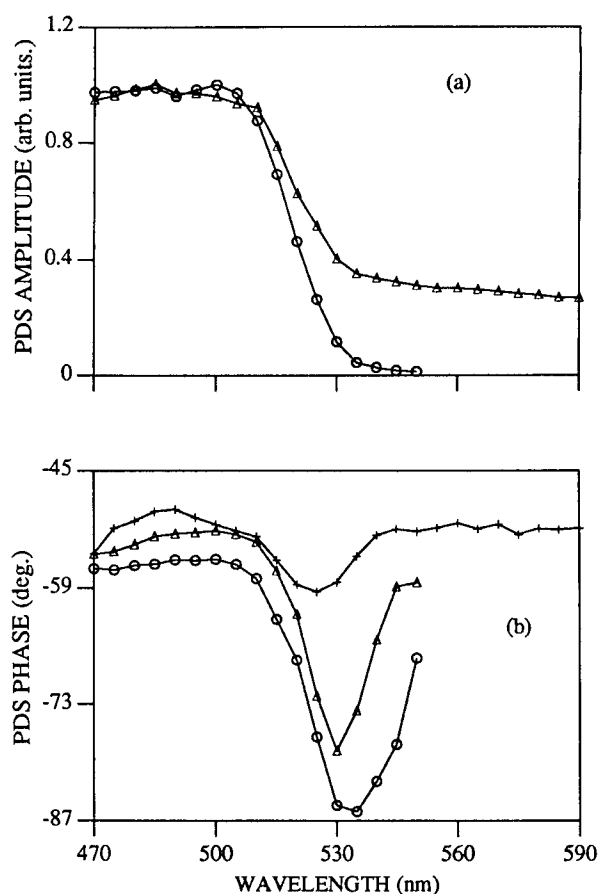


FIG. 13. PDS spectra of LR-CdS, under various biases, in 0.01 M PS; 25 Hz; (a) amplitude, -1.13 (o) and $+1.12$ (Δ) V/SCE, and (b) phase, -1.13 (o), -0.10 (Δ), and $+1.12$ (+) V/SCE.

more positive, the PDS signal will increase, more so in spectral regions where the quantum efficiency is greatest. A good example of this behavior is depicted in Fig. 12 (Ga-CdS in 0.05 M PS): As the bias was increased from -1.51 to $+2.19$ V/SCE, the wavelength of the peak PDS signal moved from 505 to 485 nm, a definite shift towards the peak PC at 480 nm. No significant bias variation was observed for the PDS phase in the superbandgap spectral region.

The magnitude of the subbandgap PDS signal relative to the superbandgap signal was usually observed to increase as a function of bias (Fig. 13a, LR-CdS in 0.01 M PS). This increase was not due to the effect described by Eq. 3, since Eq. 3 actually predicts that the relative subbandgap signal should decrease, not increase, as the bias is increased. The nature of the subbandgap PDS signal enhancement was clarified by an analysis of the associated PDS phase spectra (Fig. 13b): Subbandgap amplitude increases were always accompanied by significant decreases in the subbandgap phase lag, indicative of a growing surface damage layer. The presence of an opaque surface layer was confirmed by visual inspection—all crystals showing a large subbandgap PDS signal were blackened on their illuminated surfaces. Karas and Ellis¹⁴ observed similar black layers when large photocurrents were passed through CdS in polysulfide solution; their analysis of the layer by Auger spectroscopy revealed the presence of a significant amount of oxygen,

leading them to believe that an oxide layer had formed. The accelerated growth of the corrosion layer at high reverse bias, where large photocurrents were present, was consistent with our earlier discussion regarding anodic photocorrosion: Corrosion is more likely to be the dominant WE process at high current densities. Overall, the PDS amplitude and phase spectra were quite sensitive to the formation of thin corrosion layers on the CdS surface.

The PC spectra can be discussed with reference to the Gartner equation:³⁰

$$I_{ph} = -qA\phi[1 - e^{-\alpha W}/(1 + \alpha L_p)] \quad (4)$$

where I_{ph} is the cell photocurrent, ϕ is the light flux, α is the absorption coefficient, A is the area of illumination, W is the depletion layer thickness, and L_p is the hole diffusion length; Eq. 4 is a simplified form of the Gartner equation for n -type materials. The Gartner equation predicts that the PC band edge should move to longer wavelength as the applied bias is made more positive—as the depletion layer becomes wider, more photons with smaller absorption coefficients will be absorbed in or near the depletion layer. Experimentally, the wavelength at which the PC was initiated (as the wavelength was decreased from subbandgap values) was independent of the applied dc bias. On the other hand, the PC spectral features at strongly absorbed wavelengths were often quite dependent upon bias: As the bias was increased from forward bias, the wavelength of the peak PC was increased, and often the relative PC at the shortest wavelength was decreased—this behavior is displayed in Fig. 14 (F-CdS in 0.01 M PS). The relative subbandgap PC showed no clear trend with respect to the bias. Overall, the Gartner equation seemed to be partially correct in predicting the behavior of the PC spectra in response to an applied dc bias.

Finally, the PC phase spectra all followed a common trend: At forward bias, close to the flatband condition, the PC phase lag showed an overall decrease as the wavelength was increased across the band edge; at the two more-positive potentials the phase lag tended to show a net increase as the wavelength was increased.

CONCLUSIONS

Our experimental study of four CdS PEC electrodes via PDS and AC photoaction spectroscopy has yielded several important results. First, PDS spectra were obtained for the four samples in distilled water. The spectra were found to be quite repeatable, and acceptable signal-to-noise ratios were obtained over the entire measurement range. Also, the relative positions of the crystal band edges could be correlated with the known donor densities. The PDS phase spectra also displayed reasonable behavior, and nonideal subbandgap data were explained by invoking the existence of absorption at the surface and/or in the backing.

When PDS measurements were carried out on an electrode supporting an appreciable current flow, certain PDS signal perturbations were observed: As the electrode current was increased (with optical excitation held constant), the PDS magnitude was seen to decrease, and the phase lag to increase—a result consistent with an in-

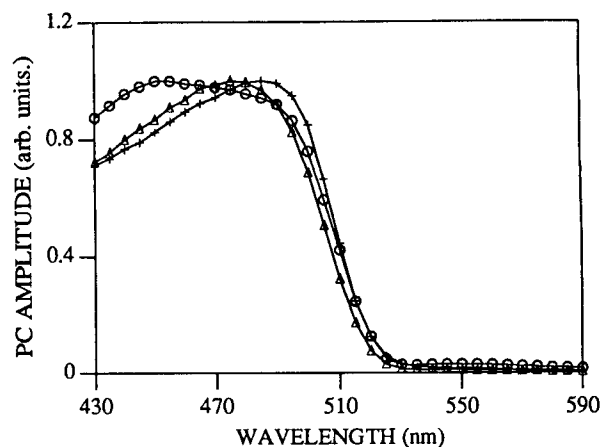


FIG. 14. PC amplitude spectra of F-CdS, under various biases, in 0.01 M PS; 25 Hz; -1.2 (o), 0.0 (Δ), and $+1.0$ (+) V/SCE; normalized by $I_0(\lambda)^{1/2}$; smoothed.

creased probe beam offset. This effect will probably limit the application of the PDS technique, as an accurate quantitative method, to currentless systems; nonetheless, PDS appeared to be a useful qualitative diagnostic tool under all conditions.

PDS and photoaction spectra were obtained under a wide range of cell conditions. The photoaction band edges were correlated with both the sample donor densities and the magnitude of applied biases, and in this respect the band edges were found to partially follow the trends predicted by the Gartner model.³⁰ The PC phase spectra were difficult to interpret owing to the lack of pertinent theoretical models, but a few coherent behavioral patterns were observed. The PV phase spectra could not be interpreted with certainty, but an apparently irregular type of behavior seemed to indicate the presence of surface corrosion layers, and another type of response observed in the 0.05 M PS may be related to large densities of electronic defects in the bandgap. Both the PV and PC phase spectra showed distinct band edge structure and may be found to yield further qualitative or quantitative information when an empirical or theoretical model for their behavior is created.

PDS spectra obtained under the application of a dc bias were found to be distorted in the superbandgap region for two reasons: First, the presence of current-induced species gradients reduced the amplitude and shifted the phase. Second, enhanced sample heating in spectral bands where the PC was high distorted the PDS amplitude spectra. These distortions did not affect the PDS signal in the subbandgap region, allowing the growth of corrosion layers to be monitored via the examination of the PDS magnitude and phase information.

Overall, both the PDS and AC photoaction methods proved to be quite useful in helping to characterize the four CdS samples. The PDS technique provided *in situ*, depth-sensitive absorption spectra which were relatively easy to interpret. The ac photoaction technique yielded both traditional carrier transport-related amplitude information and difficult-to-interpret phase data. In addition, our experiments were useful in helping to assess the application of the PDS technique to active PEC systems: Except for the species gradient effect, the PDS probe was quite reliable. Regarding the question of sys-

tem invasiveness, as noted, the HR-CdS PC spectra were found to be affected by the presence of the He-Ne probe beam.

ACKNOWLEDGMENTS

The authors wish to acknowledge the partial support of the Ministry of Energy, Mines, and Resources (EMR Canada) through an equipment loan from the Center for Hydrogen and Electrochemical Studies (CHES). Partial financial support by the Natural Sciences and Engineering Research Council of Canada (NSERC) and the Ontario Laser and Light-wave Research Center (OLLRC) is gratefully acknowledged.

1. A. B. Ellis, S. W. Kaiser, and M. S. Wrighton, *J. Amer. Chem. Soc.* **98**, 6855 (1976).
2. A. B. Ellis, S. W. Kaiser, J. M. Bolts, and M. S. Wrighton, *J. Amer. Chem. Soc.* **99**, 2839 (1977).
3. D. Dutton, *Phys. Rev.* **112**, 785 (1958).
4. D. G. Thomas, J. J. Hopfield, and M. Power, *Phys. Rev.* **119**, 570 (1960).
5. M. Cardona and G. Harbeke, *Phys. Rev.* **137**, A1467 (1964).
6. A. L. Fahrenbruch and R. H. Bube, *Fundamentals of Solar Cells: Photovoltaic Solar Energy Conversion* (Academic Press, New York, 1983).
7. J. L. Boone and G. Cantwell, *J. Appl. Phys.* **57**, 1171 (1985).
8. S. R. Morrison, *Electrochemistry at Semiconductor and Oxidized Metal Electrodes* (Plenum Press, New York, 1980).
9. *Photoacoustic and Thermal Wave Phenomena in Semiconductors*, A. Mandelis, Ed. (North-Holland, New York, 1987).
10. A. Mandelis and E. K. M. Siu, *Phys. Rev. B* **34**, 7209 (1986).
11. J. Powderly, Eagle-Pitcher Inc., Miami, Oklahoma, private communication.
12. R. H. Bube and S. M. Thomsen, *J. Chem. Phys.* **23**, 15 (1955).
13. R. W. Smith, *Phys. Rev.* **97**, 1525 (1955).

14. B. R. Karas and A. B. Ellis, *J. Amer. Chem. Soc.* **102**, 968 (1980).
15. G. Hodes, *J. Photochem.* **29**, 243 (1985).
16. S. Licht and J. Manassen, *J. Electrochem. Soc.* **132**, 1076 (1985).
17. A. Mandelis, *J. Appl. Phys.* **54**, 3404 (1983).
18. A. Mandelis, W. Lo, and R. E. Wagner, *Appl. Phys. A* **44**, 123 (1987).
19. J. Fesquet, B. Girault, and M. D. M. Razafindrandriatsimaniry, *Appl. Opt.* **23**, 2784 (1984).
20. K. Yamashita, H. Kasahara, K. Yamamoto, and K. Abe, *Jpn. J. Appl. Phys. Supplement* **21-3**, 107 (1982).
21. T. Hata, T. Hatsuda, M. Kawakami, and Y. Sato, *Jpn. J. Appl. Phys. Supplement* **24-1**, 204 (1985).
22. R. E. Wagner and A. Mandelis, unpublished data.
23. Y. Y. Gurevich and Y. V. Pleskov, in *Semiconductors and Semimetals*, R. K. Willardson and A. C. Beer, Eds. (Academic Press, New York, 1983), Vol. 19, Chap. 4.
24. A. Heller and B. Miller, *Electrochim. Acta* **25**, 29 (1980).
25. *CRC Handbook of Chemistry and Physics, 1979-80* (CRC Press, Boca Raton, Florida, 1980), p. F-62.
26. J. H. Lienhard, *A Heat Transfer Textbook* (Prentice-Hall, Englewood Cliffs, New Jersey, 1981).
27. A. Mandelis and B. S. H. Royce, *Appl. Opt.* **23**, 2892 (1984).
28. A. Dorthe-Merle, J. P. Morand, and E. Maurin, *Tech. Digest, 4th Int. Top. Meeting on Photoacoustic, Thermal, and Related Sciences MD5.1* (1985).
29. J. Pawliszyn, M. F. Weber, M. J. Dignam, A. Mandelis, R. D. Venter, and S. M. Park, *Anal. Chem.* **58**, 236 (1986).
30. W. W. Gartner, *Phys. Rev.* **116**, 84 (1959).
31. H. Gerischer, M. Lubke, and B. Bressel, *J. Electrochem. Soc.* **130**, 2112 (1983).
32. J. P. Roger, D. Fournier, A. C. Boccara, R. Noufi, and D. Cahen, *Thin Solid Films* **128**, 11 (1985).
33. A. Fujishima, Y. Maeda, K. Honda, G. H. Brilmyer, and A. J. Bard, *J. Electrochem. Soc.* **127**, 840 (1980).

A Study of Natural and Synthetic Rubies by PIXE

S. M. TANG,* S. H. TANG, K. F. MOK, A. T. RETTY, and T. S. TAY

Department of Physics, National University of Singapore, Singapore 0511 (S.M.T., S.H.T.); Department of Chemistry National University of Singapore, Singapore 0511 (K.F.M.); Retty Enterprises, 3 Lengkok Merak, Singapore 1024 (A.T.R.); and Elvin Gems Pte. Ltd., 79 Jalan Taman, Singapore 1232 (T.S.T.)

Trace element analysis of 160 natural- and synthetic rubies was carried out by using the technique of proton-induced x-ray emission (PIXE). It was found that the natural rubies contained more and higher concentrations of impurities than did their synthetic counterparts. Our results suggest that vanadium and iron are good indicators for separating synthetic rubies from the natural ones. The concentration of chromium is also helpful in many cases for source identification.

Index Headings: Proton-induced x-ray emission (PIXE); Gemstones.

INTRODUCTION

Ruby, a red corundum, is one of the most appreciated gems that have been used as jewelry ornamentation by human kind for many centuries. It is a mineral of very limited distribution, and it commands a higher price than many other colored gemstones. The best known country

where very fine-quality rubies occur is Burma. Thailand is another major source of quality rubies and is, in fact, the world's busiest ruby trade center at present. Rubies also occur in Sri Lanka, India, Kenya, Pakistan, Afghanistan, and some other countries, but they are not usually of such good color as the Burmese and Thai stones.

As fine-quality gemstones are rare and expensive, their substitution with imitations and synthetics for ornamental purpose follows naturally. The historical record¹ reveals that early Egyptians made glass beads to imitate natural gemstones. However, it was not until the end of the 19th century that duplication of natural gems became a reality. The first successful commercial synthesis of ruby was achieved by Auguste Veneuil of France shortly after 1900; his technique is known as the flame fusion method.¹ Since the 1960s, another process, called the flux method, developed originally by C. Fremy in 1877, has also been used to grow synthetic rubies for commercial

Received 24 May 1988; revision received 15 August 1988.

* Author to whom correspondence should be sent.